teraction as the temperature is raised. This destabilization of the α-peptide in solution accounts for the decrease in productive interaction between the α- and β-peptides in vitro (Figure 2).

If, as the results in this paper suggest, the N-terminal α-peptide portion of the PA precursor folds in the early stages of biosynthesis in vivo of the whole chain allowing the β-peptide portion to fold and rapidly associate with the α-peptide, the temperature dependence of PA processing observed in vivo could result from the temperature-induced instability of folding of the α-peptide moiety. This constitutes a further example of a temperature-dependent block in protein folding in vivo [cf. King (1986)].

ACKNOWLEDGMENTS

The contribution of Dr. R. Virden in suggesting the experiment using PMSF as active-site titrant is acknowledged. We thank A. Böck, H. Burtscher, K. R. Hejnaes, C. Keilman, G. Schumacher, D. Sizmann, C.-L. Tsou, and R. Virden for useful discussions and for exchange of information prior to publication. We thank Susan Lee for preparation of the manuscript.

REFERENCES

Ahmad, F., & McPhie, P. (1978), *Int. J. Pept. Protein Res. 12*, 155–163.
Anfinsen, C. B. (1967) *Harvey Lect. 61*, 95–116.
Böck, A., Wirth, R., Schmid, G., Schumacher, G., Lang, G., & Buckel, P. (1983a) *FEMS Microbiol. Lett. 20*, 135–139.
Böck, A., Wirth, R., Schmid, G., Schumacher, G., Lang, G., & Buckel, P. (1983b) *FEMS Microbiol. Lett. 20*, 141–144.
Daumy, G. O., Danley, D., & McColl, A. S. (1985) *J. Bacteriol. 163*, 1279–1281.
Frank, B. H., & Chance, R. E. (1983) *Münch. med. Wschr. 125* (Suppl. 1), 14–20.
Givol, D., DeLorenzo, F., Goldberger, R. F., & Anfinsen, C. B. (1965) *Proc. Natl. Acad. Sci. U.S.A. 53*, 676–684.
Gomori, G. (1955) *Methods Enzymol. 1*, 140–146.
King, J. (1986) *Bio/*Technology, *4*, 297–303.
Kutzbach, C. & Rauenbusch, E. (1974) *Hoppe-Seyler's Z. Physiol. Chem. 354*, 45–53.
Lah, T., Drobnic-Košorok, M., Turk, V., & Pain, R. H. (1984), *Biochem. J. 218*, 601–608.
Lindsay, C. D., & Pain, R. H. (1990) *Eur. J. Biochem. 192*, 133–141.
Pain, R. H. (1978) in *Characterisation of Protein Conformation and Function* (Franks, F., Ed.) pp 19–36, Symposium Press, London.
Pain, R. H., Lah, T., & Turk, V. (1985) *Biosci. Rep. 5*, 957–967.
Privalov, P. L., Mateo, P. L., Khechinashvilli, N. N., Stepanov, V. M., & Revina, L. P. (1981) *J. Mol. Biol. 152*, 445–464.
Sizmann, D., Keilmann, C., & Böck, A. (1990) *Eur. J. Biochem. 192*, 143–151.
Tang, J.-G., & Tsou, C.-L. (1990) *Biochem. J. 268*, 429–435.
Taniuchi, H. (1970) *J. Biol. Chem. 245*, 5459–5468.
Valle, F., Balbás, P., Merino, E., & Bolivar, F. (1991) *Trends Biochem. Sci. 16*, 36–40.

Solution Structure of Fe(II) Cytochrome *c*551 from *Pseudomonas aeruginosa* As Determined by Two-Dimensional ^{1}H NMR†

David J. Detlefsen,‡ V. Thanabal,‡ V. L. Pecoraro,§ and Gerhard Wagner*,‡

Department of Biological Chemistry and Molecular Pharmacology, Harvard Medical School, 240 Longwood Avenue, Boston, Massachusetts 02115, and Department of Chemistry, The University of Michigan, Willard H. Dow Laboratory, Ann Arbor, Michigan 48109

Received April 8, 1991; Revised Manuscript Received July 3, 1991

ABSTRACT: The solution structure of Fe(II) cytochrome *c*551 from *Pseudomonas aeruginosa* based on 2D ^{1}H NMR data is reported. Two sets of structure calculations were completed with a combination of simulated annealing and distance geometry calculations: one set of 20 structures included the heme–peptide covalent linkages, and one set of 10 structures excluded them. The main-chain atoms were well constrained within the two structural ensembles (1.30 and 1.35 Å average RMSD, respectively) except for two regions spanning residues 30–40 and 60–70. The results were essentially the same when global fold comparisons were made between the ensembles with an average RMSD of 1.33 Å. In total, 556 contraints were used, including 479 NOEs, 53 volume constraints, and 24 other distances. This report represents the first solution structure determination of a heme protein by 2D ^{1}H NMR and should provide a basis for the application of these techniques to other proteins containing large prosthetic groups or cofactors.

Cytochromes are heme (iron porphyrin) proteins generally involved in some type of electron transfer process. Soluble cytochromes are single polypeptides containing one heme group with the iron alternating between Fe(II) and Fe(III) in the electron transfer process. *c*-type cytochromes are distinct in two respects: the heme is covalently attached by two thioether linkages arising from cysteine residues near the N-terminus, and the axial iron ligands are sulfur from methionine and nitrogen from histidine. The spectroscopic properties of *c*-type cytochromes, and heme proteins in general, are well understood (Ochiai, 1977).

Cytochrome *c*551 from *Pseudomonas aeruginosa* is a small bacterial *c*-type cytochrome of 82 residues. We have previously reported the spin system identification, sequential assignments,

†This study was supported by the NSF (BBS-8615223) and the NIH (Grant 1GM38608).
* Author to whom correspondence should be addressed.
‡Harvard Medical School.
§University of Michigan.

0006-2960/91/0430-9040$02.50/0

and secondary structure of Fe(II) cytochrome *c*551[1] (Detlefsen et al., 1990). These results were essentially in agreement with a similar study on Fe(II) *c*551 (Chau et al., 1990). In this paper, we report the results of structure calculations on Fe(II) *c*551. This effort is unique in two respects: (1) it is the first complete solution structure determination of a heme protein by NMR, and (2) it provides a guide to NMR solution structure determinations of proteins with large prosthetic groups, cofactors, and bound substrates. In addition, this report may generate renewed interest in *c*551 and its function as an electron transfer agent with its proposed physiological partners: azurin and cytochrome oxidase (Horio, 1958; Wood, 1978). Recent efforts have shown that NMR is a useful tool in defining surface sites that are important in protein–protein interactions during electron transfer processes (Bagby et al., 1990; Whitford et al., 1990), and similar studies on Fe(II) *c*551 are now possible with the results of this work.

Materials and Methods

Data Collection and Processing. All ^{1}H NMR data were collected and processed as previously described (Detlefsen et al., 1990) on freshly reduced samples in 0.05 M phosphate buffer (pH 6.8) at 25 °C.

NOE Quantification. NOE intensities were determined by counting contour levels on a 75-ms NOESY spectrum collected in water. Distances were quantified by using an internal calibration procedure based on three assumptions: (1) that no significant spin diffusion was encountered in the 75-ms mixing time spectra, (2) the classes of backbone NOE cross peaks selected (vide infra) sampled the complete range of distances conformationally possible, and (3) that line widths were similar to allow for this type of quantification.[2] The calibration involved counting contours on the 75-ms NOESY spectrum for sequential $d_{\alpha N(i,i+1)}$ and intraresidue $d_{N\alpha(i,i)}$ cross peaks. These distances have been reported to span 2.20–3.55 and 2.16–2.85 Å, respectively, according to conformational flexibility in the ϕ and ψ angles (Wüthrich, 1986). Therefore, the range of contours for $d_{\alpha N(i,i+1)}$ and $d_{N\alpha(i,i)}$ cross peaks was assumed to span 2.16–3.55 Å. Fixing the most distant pair to 3.55 Å with the fewest contours and the closest pair to 2.16 Å with the most contours, the expression relating NOE intensity to distance can be solved for two proportionality constants (c). The average of these two constants was used in the following expression to convert NOE intensities to distances

$$r_{\text{Å}} = c[\text{NOE}]^{(-1/6)}$$

where c = a proportionality constant and $[\text{NOE}] = 1.4^{(\text{number of contours})}$. The substitution of contours for NOE intensity was made since the spectrum was plotted on the $\log_{1.4}$ scale (subsequent higher contour levels were 1.4 times the previous contour level). Contours were counted on plots prepared on a scale of 0.1 ppm per centimeter or 0.05 ppm per centimeter to ±2 levels. From this point, there were two possible ways to proceed. The counted number of levels −2 contours and +2 contours could have been used to set the upper and lower bounds, respectively. Otherwise, the upper bounds could have been set to the number of contours −2 and the lower bounds set to van der Waals contact distance. It was felt that the later was more conservative; therefore, it was the approach used. The upper bounds were set to 5 Å where the number of contours counted were one or two and when the cross peak could only be observed in a 150-ms NOESY spectrum. No stereospecific assignments were made. In cases involving an NOE cross peak with one proton of a stereopair (e.g., methylene protons), appropriate distances were added (assuming the maximum possible allowed distance between the heavy atom and the nonbonded proton involved in the NOE cross peak), and the distance constraint was set to the nearest stereospecifically unambiguous heavy atom. These corrections included distance additions of 1.1 Å for methylene protons referencing to the carbon, 2.1 Å for (2,6) and (3,5) ring protons for Phe and Tyr referencing to the (1) and (4) ring carbons, respectively, 2.4 Å for Val and Leu methyl groups referencing to the β and γ carbons respectively, and 1.0 Å for stereospecific methyls referencing to the methyl pseudoatom. A 0.5-Å addition was included for NOE cross peaks involving methyl protons. Where NOE cross peaks were observed for both spins of a stereopair, the distances for both were set to that calculated for the weaker (fewer contours) cross peak.

Distance and Other Constraints. A total of 479 NOE distance constraints were used in all calculations, including 24 intraresidue, 179 sequential, 88 medium-range, and 184 long-range connectivities. Excluding the intraresidue constraints, there was an average of over 5 constraints per residue. Other constraints from data on slowly exchanging backbone amide protons and medium-range NOE cross peaks [$d_{\alpha N(i,i+3)}$] were used to fix hydrogen-bond distances between backbone amide protons and carbonyl oxygens. Volume constraints were included to aid in maintaining planarity in the aromatic rings. A total of 16 such constraints were used for the heme and included only substituent pyrole rings and bridge meso carbons. In all, there were 556 constraints used: 479 NOEs, 24 other distances, and 53 volumes.

Structure Calculations and Analysis. Structure calculations were accomplished with a new distance geometry program, DG-II, which utilizes a combination of simulated annealing and distance geometry (Havel, 1991). A heme library entry was created for DG-II by using the coordinates from the 1.6-Å X-ray crystal structure of Fe(II) *c*551 (Matsuura et al., 1982). Two sets of calculations were completed: (1) 20 structures were determined by using covalent bond distances for the cysteinyl thioether linkages to the heme edge and axial iron–sulfur and iron–nitrogen from the X-ray structure (Matsuura et al., 1982) and (2) 10 structures without these covalent constraints. All calculations were completed on a Sun SparcStation 2 (64 Mb RAM) requiring approximately 3 days of CPU time per 20 structures. INSIGHTII (BioSym) was used to generate the figures and calculate backbone RMSDs.[3]

Results

Structures with Covalent Linkages. A total of 20 structures were calculated by using X-ray distances for the thioether linkages and Fe(II) axial ligation, and 18 structures were selected for further analysis on the basis of the final gradient error after annealing and minimization. Two structures were rejected since the final gradient errors were an order of magnitude greater than the other 18 and were not considered further. Visual inspection of these two showed that they were roughly mirror images (global fold enantiomers) of the other

[1] Abbreviations: NMR, nuclear magnetic resonance; 2D, two dimensional; NOE, nuclear Overhauser effect; NOESY, 2D NOE spectroscopy; Fe(II) *c*551, Fe(II) cytochrome *c*551; RMSD, root-mean-square deviation.

[2] It is important to consider line width in any quantification scheme that does not measure peak volume. The distinction between a broad peak and a weak peak may be impossible to make when counting contours. Cross peaks used to derive the constant were of similar line width as judged by examining cross peak appearance at low plotting levels justifying the calibration scheme discussed.

[3] All RMSDs were calculated for main-chain atoms, including C_α, C, and N.

FIGURE 1: Superpositioning of main-chain atoms for 10 structures that included covalent linkages to the heme. The structure with the lowest residual error after minimization was chosen as the fixed structure.

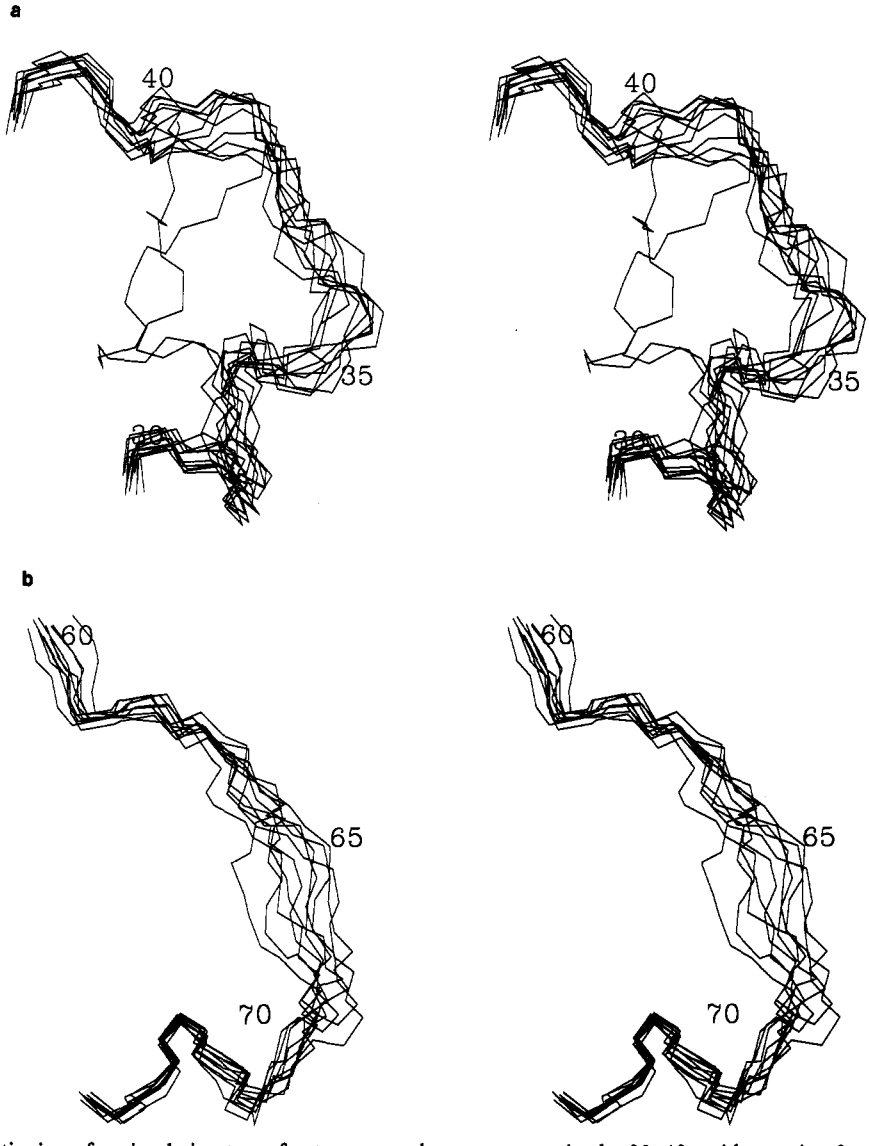

FIGURE 2: (a) Superpositioning of main-chain atoms for two anomalous structures in the 30–40-residue region from calculations including covalent linkages to the heme. The 10 structures from Figure 1 are included for reference. (b) Same as panel a for the 60–70-residue region.

18 with partial left-handed helices. A superpositioning of the main-chain atoms is shown for 10 of these structures in Figure 1. The average RMSD[4] for these 10 structures was 1.30 Å (ranging from 0.98 to 1.58 Å). Figure 1 shows that the main-chain atoms are well constrained except for two regions at residues 30–40 (Figure 2a) and residues 60–70 (Figure 2b). The other eight structures (not shown) exhibited the same global fold as those in Figure 1. The deviations (and cause for the higher gradient errors) were localized to the 30–40- and 60–70-residue regions. This was evident by a visual inspection of the structures and an examination of residual NOE violations.

Structures without Covalent Linkages. Ten structures were calculated after removing the four heme-peptide covalent

[4] Average RMSDs were calculated by determining the RMSDs for all possible unique superpositionings between two ensembles (or one structure with an ensemble) and taking the average of these values.

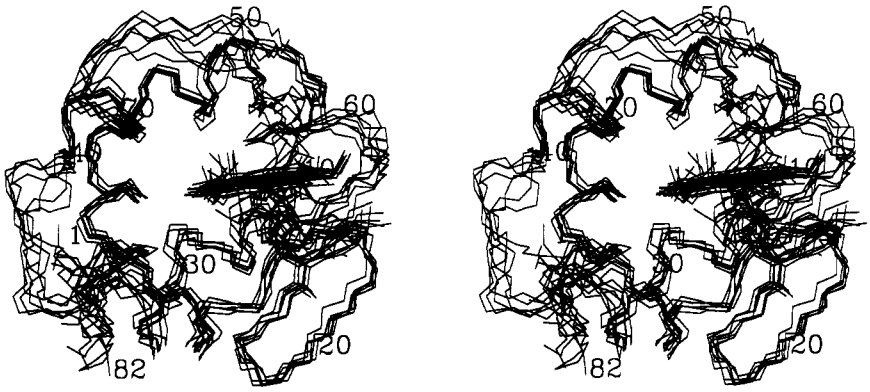

FIGURE 3: Superpositioning of main-chain atoms for seven structures determined that excluded heme–peptide covalent linkages. The structure with the lowest residual error after minimization was chosen as the fixed structure.

linkages. Seven structures were selected on the basis of the final gradient error for further analysis. One structure was discarded because of a high residual error and since an examination of this structure showed that the C-terminal helix had crossed through a portion of the molecule. The other two were discarded because of larger deviations and residual violation in the 30–40- and 60–70-residue regions. The superpositioning of the seven selected structures is shown in Figure 3. It can be seen that there is agreement for the main chain; removing the heme–peptide covalent linkages did not (at least at this level of analysis) introduce any noticeable structural uncertainty within the set. The average RMSD for these structures was 1.35 Å (ranging from 1.15 to 1.62 Å). Although the average RMSD for this set was slightly higher than for the ensemble that included the heme–peptide covalent linkages, it is unlikely that this deviation is significant. A comparison of the main-chain atoms between the two sets of calculated structures indicated that the global fold is identical with the average RMSD between the sets of 1.33 Å.

The average iron–nitrogen and iron–sulfur distances from these structures were 4.20 (1.97) and 3.70 (2.35) Å, respectively, as compared to the values defined by the X-ray structure (Matsuura et al., 1982) indicated in parentheses.

Discussion

We have determined the structure of Fe(II) cytochrome *c*551 in solution. A comparison of the structures calculated with and without the covalent heme–peptide linkages as constraints showed no significant variation in the global fold. The average RMSDs for main-chain atoms were virtually identical between the two sets of structure determinations when main-chain RMSD comparisons were made. It is noteworthy that the axial ligand side-chain conformations were not highly constrained in the ensemble that excluded the heme–peptide covalent linkages. The number of axial ligand to heme NOE cross peaks are 3 and 13 for His 16 and Met 61, respectively. An inspection of the residual NOE violation listings showed that these constraints were not in violation for any of the structures. However, there is enough structural flexibility in the methionine χ angles to allow for movement of the sulfur away from the iron and yet satisfy the NOE constraints. The χ angle correlations (vide infra) showed that removal of the iron–sulfur distance introduced more variability in Met 61 side chain (χ_1 = 138, 0.63; χ_2 = 81, 0.51; and χ_3 = −38, 0.19, where the first number is the angle and the second is the angle correlation). The inability to more accurately define the iron–nitrogen distance may be the result of relatively few constraints linking this axial ligand to points around the heme. Thus, it was not surprising that the distances obtained for the iron–sulfur (3.7 Å) and iron–nitrogen (4.2 Å) did not come closer to the X-ray values (Matsuura et al., 1982). It seems likely that the constraints were simply not sufficient to define a consensus conformation for the axial ligands allowing for accurate independent iron–sulfur and iron–nitrogen distance determinations.

Table I: Comparison of Dihedral Angles for Iron Axial Ligands His 16 and Met 61

	His 16			Met 61		
angle	X-ray[a]	NMR[b]	NMR[c]	X-ray[a]	NMR[b]	NMR[c]
ϕ	−132		−104	−92		−71
ψ	148		−122	117		130
χ_1	−70		−94	176	166	153
χ_2	100		86	166	148	151
χ_3				47	40	56

[a] Data from the X-ray structure of Fe(II) *c*[551] (Matsuura et al., 1982). [b] Data from previous NMR work (Senn et al., 1984). [c] Results of this study.

Table I shows the dihedral angle assignments for the axial ligands His 16 and Met 61 as determined by several studies. It can be seen that the angles for Met 61 agree. The side-chain and ϕ dihedral angles for His 16 are also nearly the same; however, the ψ dihedral angles are dissimilar. This does not necessarily constitute a conflict; rather it may be that the His 16 ψ is not well defined by the NMR data. In fact, the ψ angle correlation (vide infra) of His 16 is low at 0.459 (Figure 7a).

There are two of other areas of general structural interest that were considered in more detail, including the local heme environment and the so-called polyproline helix. Figure 4 shows an expansion of the region around the heme for structures that included the heme–peptide covalent linkages from Figure 1. It can be seen from this figure that even though the heme was not considered in RMSD superpositioning, the hemes from different structures superimpose well. The position of the axial ligand side chains (Figure 4) visually confirm the data of Table I. Figure 5 shows a stretch of residues from 55 to 63 that contains four prolines and the axial ligand Met 61. The side chains of prolines 58 and 60 appear somewhat disordered. This is likely due to lack of NOE constraint data on this segment.

Figure 6 shows two plots that were used to judge the quality of structures presented. An evaluation was made considering only the average residual violations (Figure 6a) and by comparing these with the total number of constraints per residue (Figure 6b). NOE cross peaks involving residues that had high values in both panels a and b of Figure 6 were rechecked on the spectra. Figure 6a indicates several areas that are consistently in violation, with the heme being the major contributor.[5] However, the heme violations must be placed in per-

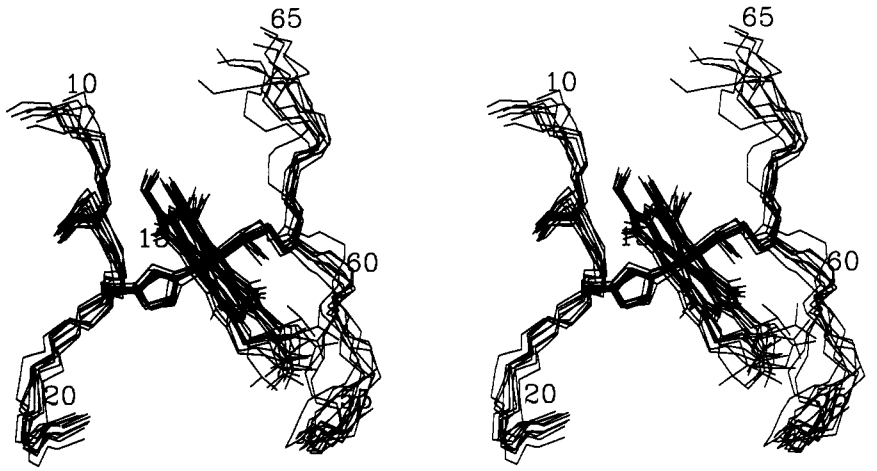

FIGURE 4: Expansion of the heme environment for the 10 structures that included heme covalent linkages. Main-chain atoms of the polypeptide are shown for residues 10–20 and 55–66. Side-chain atoms are shown for iron axial ligands His 16 and Met 61.

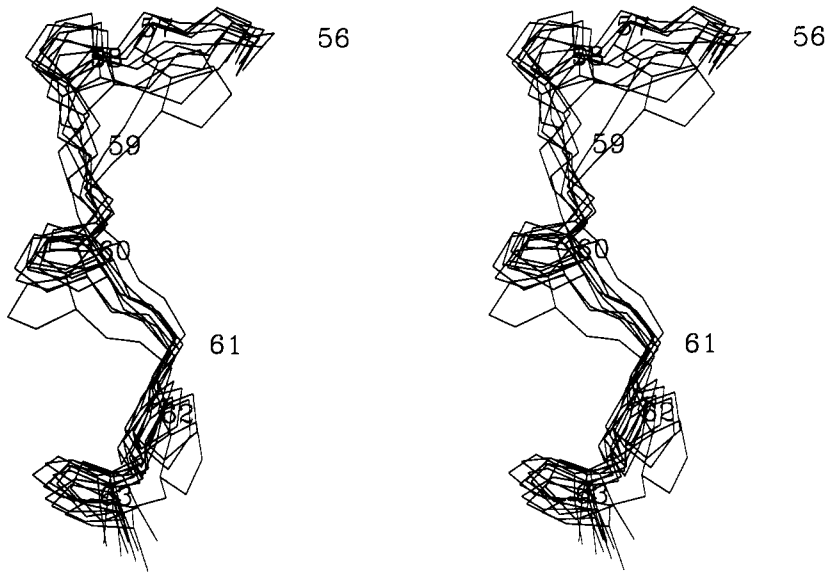

FIGURE 5: Expansion of the structures from residue 55 to 63 for 10 structures that included heme covalent linkages. This region contains four prolines and is sometimes referred to as a polyproline helix.

spective, considering the number of NOE cross peaks per residue (Figure 6b). That is, since there are more NOE cross peaks involving heme resonances, there can be more violations. Another prominent region in violation in Figure 6b is Val 78. There are two constraints that were violated in all ten structures between a Val 78 methyl to heme 1 methyl group and the same Val 78 methyl to the heme 7 propionate. A reexamination of the NOESY spectrum showed that the former NOE cross peak was well resolved while the later was potentially ambiguous in a region where several H_α resonances lie. The last region of significant violation was around Ala 14. There were three consistent violations in all ten structures between Ala 14 NH to Val 13 H_α and H_β. A reexamination of the spectra showed that these cross peaks were slightly overlapping but resolvable at two temperatures (15 and 25 °C). These violations may be due to mobility.

Although some information about the heme group from the X-ray structure of Fe(II) *c*551 was incorporated into this work, it seems unlikely that this biased the solution structure determination. The heme was simply considered as another residue with a characteristic structure and bonding geometry. This approach appears to be adequate to a first approximation as indicated by the results of this study. A logical extension of this approach would be to allow for some bond length and bond angle variations in the structure calculations where there may be some uncertainty in prosthetic group conformation.

Figures 7 and 8 are representations showing how well the dihedral angles ϕ and ψ are defined. Figure 7a,b shows dihedral angle correlation diagrams where, for each residue, we have represented the angle ϕ_i of structure i by a two-dimensional vector $\mathbf{r}(\phi_i)$ of length 1 and phase ϕ_i. These vectors were summed up for all structures calculated and divided by the number structures. Thus, if the ϕ_i angles are the same in all structures, we have a value of 1.0; if they are randomly distributed, we have a value of 0. The data are shown for the dihedral angles ϕ and ψ in Figure 7, panels a and b, respectively. A comparison of these two panels shows that, in most cases, a poorly defined angle ϕ_i is correlated with a poorly defined angle ψ_{i-1}. This means that the overall fold of the backbone is well defined, but the orientation of the plane of the peptide bond is not defined.

Figure 8a is a Ramachandran plot of all 10 structures that included the heme–peptide covalent linkages. Given that these structures have not been subjected to any energy minimization,

[5] The largest individual violation for any of the 10 structures that included the heme–peptide covalent linkages was 0.39 Å. A total of six violations greater than 0.1 Å appeared consistently in all 10 structures.

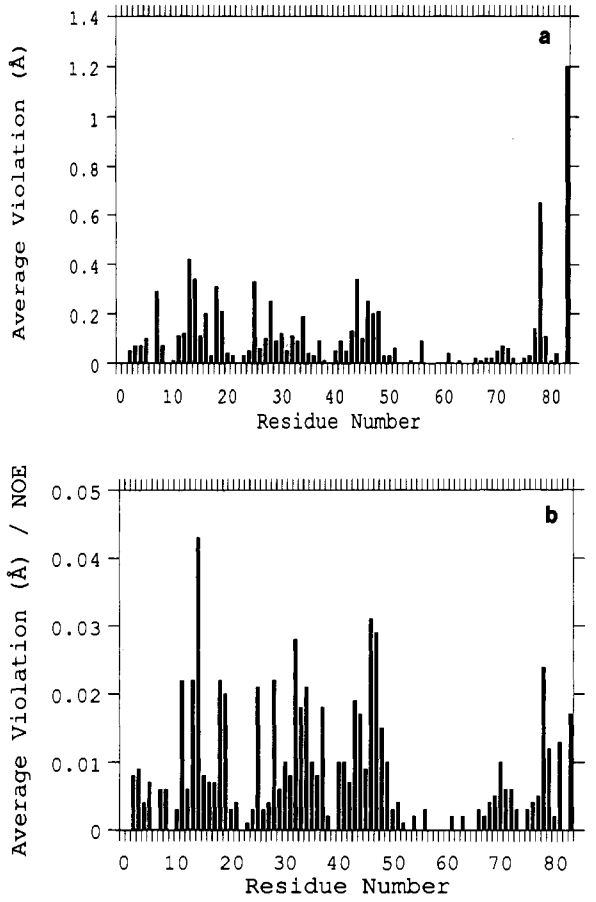

FIGURE 6: (a) Plot of the average violation per residue for 10 structures that included heme–peptide covalent linkages. (b) Plot of the average violation divided by the total number of NOE cross peaks (sum of sequential, medium-, and long-range NOEs) versus residue number for 10 structures that included heme–peptide covalent linkages.

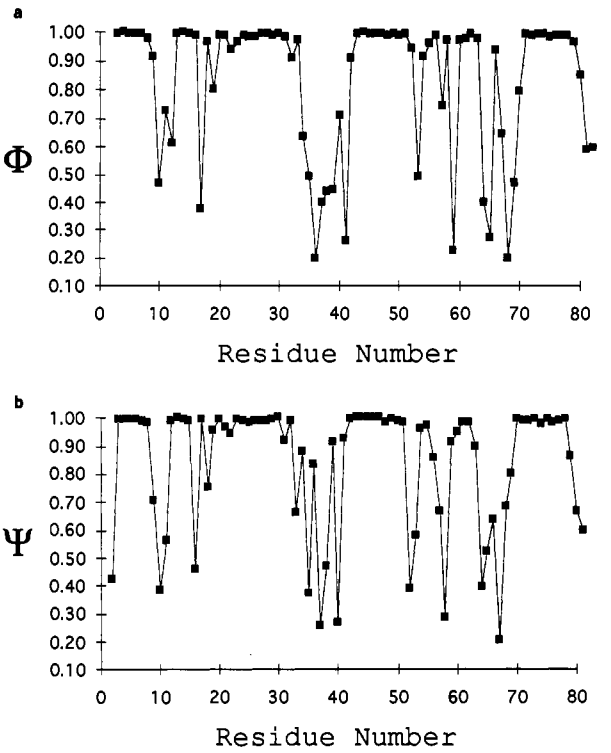

FIGURE 7: (a) ϕ correlation diagram for 10 structures that included heme–peptide covalent linkages. The Y axis value is the average vectorial sum (each angle is a unit vector) of the ϕ dihedral angles. Values nearer to 1 indicate a well-defined angle. A completely random distribution of the angle would result in a value of 0. The X axis is the residue number. (b) Same as in panel a except for the ψ angles.

the ϕ–ψ map appears reasonable. The helical regions are clearly visible by the grouping of points in the upper portion of the lower left quadrant. Cytochrome *c*551 contains seven glycines that can lead to points on Figure 8a with positive ψ angles.

Figure 8b shows the Ramachandran plot for all residues that had both ϕ and ψ correlations of greater than 0.9 (Figure 7a,b). These residues are well constrained by the NMR data used for structure calculations as indicated by the agreement within the ensemble for these values. It is of interest to see where these residues fall on the ϕ–ψ map, especially since there was no backbone dihedral angle information included in the calculations. It can be seen that all of these residues fall within (or very near to) the allowed regions.

The solution and crystal structures agree on the global fold with an average main-chain RMSD of 1.90 Å. This value was calculated by comparing the 10 structures shown in Figure 1 with the X-ray structure. Three areas were identified as major contributors to the increased average RMSD between X-ray and solution structures as compared to average RMSDs within the solution structure ensemble. Two of the regions were previously discussed (residues 30–40 and 60–70). The contribution of these areas to increasing the average RMSD is not surprising since the solution structures are variable in these areas. It is noteworthy that the temperature factors for the crystal structure are highest (peaking at Ala 35) in the 30–45-residue region (Matsuura et al., 1982). The last area that contributed significantly to increasing the average RMSD was near the beginning of the N-terminal helix. This might be explained by the general observation that often the most poorly defined regions in protein solution structures are polypeptide termini.

Since this is the first solution structure of a heme protein by NMR methods, methodology needed to be developed to incorporate the heme in structure calculations. Our approach was to treat the heme simply as another residue. A heme DG-II library entry was created by using the X-ray crystal structure coordinates. In addition, 27 chirality constraints that consisted of interconnecting sets of four atoms around the aromatic portion of the heme were included to maintain planarity. The first set of calculations included the heme–peptide covalent linkages. The second set excluded them and served as a control to the first set. The results of the two were essentially identical (RMSD of the main chain for the two ensembles was 1.33 Å). Even though the heme was not considered in RMSD superpositions between the two sets, the location of the heme was the same (within the resolution of the structures) with respect to the polypeptide. These results argue that the covalent linkages are not necessary to properly orient the heme, not surprisingly since there were many NOEs between the heme and the polypeptide. The approach we made for solving a structure of a protein with a prosthetic group may be generally applicable. The strategy we have used can be summarized as (i) coordinates on the structure of the prosthetic group were obtained, (ii) appropriate constraints were included to maintain the geometry within the prosthetic group, and (iii) where covalent linkages between the polypeptide and prosthetic group exist, two sets of calculations were performed including and excluding the covalent bonds.

In summary, the results of this work show that established methods for solution structure determination by NMR methods can be applied to proteins with large prosthetic groups. Heme proteins are particularly suited owing to the well-defined structure of the porphyrin. A detailed comparison

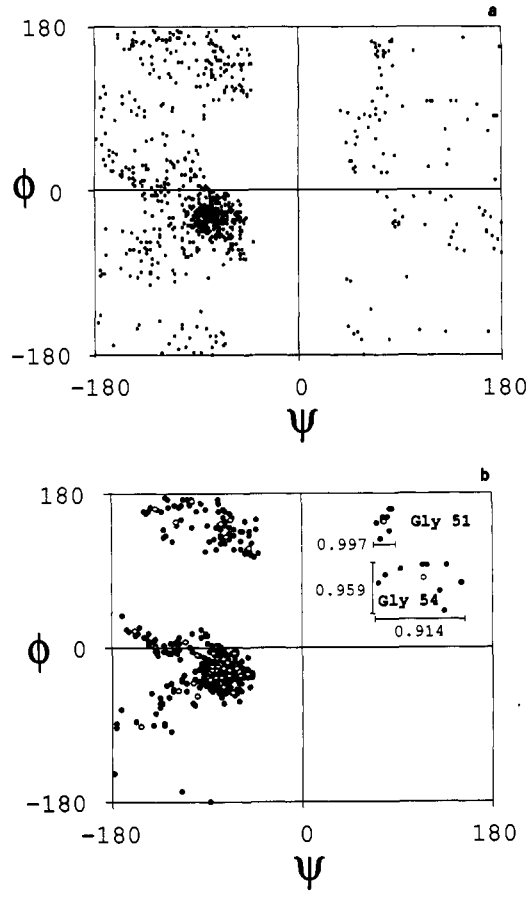

FIGURE 8: (a) Ramachandran plot for 10 structures that included heme–peptide covalent linkages. (b) Same as in panel a except only residues that had both ϕ and ψ correlations greater than 0.9 were included. The closed circles indicate the points for individual structures, while the open circles indicate average values. ϕ and ψ correlations for Gly 51 and Gly 54 are shown to indicate what correlations between 0.9 and 1 look like.

of the NMR solution structure versus the X-ray crystal structure was not included since it was felt that a more highly refined solution structure would be required to make such comparisons meaningful. This is especially true for side-chain conformations. A discussion of structure versus physiological function was also not included for the same reason. Further studies are in progress to aid in defining side-chain positions (χ_1 angles) and refine the areas of the main chain that are in poor agreement.

ACKNOWLEDGMENTS

We thank Tim Havel for providing us with a copy of DG-II and for assistance in using the program. We also thank Sven Hyberts for the use of a program to construct Figures 7 and 8.

SUPPLEMENTARY MATERIAL AVAILABLE

Listing of all NOE constraints used for structure calculations as well as the other distance constraints used. Contour levels were counted for each of these cross peaks in a 75-ms NOESY spectrum. Distances were quantified as described under Materials and Methods. Each line represents a distance constraint between atom 1 and atom 2, where the upper bounds distance was fixed to R (Å). The distances were used to the hundreth of an angstrom to avoid rounding errors and are not intended to imply precision. Other distances at the end of the supplementary materials are data used for covalent linkages between the heme and peptide as well as hydrogen-bond distances derived from knowledge of proton exchange rates and medium-range NOE patterns (11 pages). Ordering information is given on any current masthead page.

REFERENCES

Bagby, S., Driscoll, P. C., Goodall, K. G., Redfield, C., & Hill, H. A. O. (1990) *Eur. J. Biochem. 188*, 413.

Chau, M.-H., Cai, M. L., & Timkovich, R. (1990) *Biochemistry 29*, 5076.

Detlefsen, D. J., Thanabal, V., Pecoraro, V. L., & Wagner, G. (1990) *Biochemistry 29*, 9377.

Havel, T. F. (1991) *Prog. Biophys. Mol. Biol. 56*, 43.

Horio, T. (1958) *J. Biochem. (Tokyo) 45*, 195.

Matsuura, Y., Takano, T., & Dickerson, R. E. (1982) *J. Mol. Biol. 156*, 389.

Ochiai, E. (1977) *Bioinorganic Chemistry*, pp 81, Allyn and Bacon, Boston, MA.

Senn, H., Billeter, M., & Wüthrich, K. (1984) *Eur. J. Biophys. 11*, 3.

Whitford, D., Concar, D. W., Veitch, N. C., & Williams, R. J. P. (1990) *Eur. J. Biochem. 192*, 715.

Wood, P. M. (1978) *FEBS Lett. 92*, 214.

Wüthrich, K. (1986) *NMR of Proteins and Nucleic Acids*, John Wiley & Sons, New York.